WARSAW UNIVERSITY OF TECHNOLOGY Index 351733
FACULTY OF CIVIL ENGINEERING
COMMITTEE FOR CIVIL AND WATER ENGINEERING
POLISH ACADEMY OF SCIENCES ISSN 1230-2945
DOI: 10.24425/ace.2026.158610
ARCHIVES OF CIVIL ENGINEERING
Vol. LXXII ISSUE 2 2026
pp. 295 –309

Research paper

Dual-column reinforced steel modular cabins in electrical infrastructure: component property and structural seismic performance

Zhixiang Liu[1], Xingfu Jin[2], Hong Mu[3], Bo Yang[4]

Abstract: This study proposes a compact seismic reinforcement strategy for stacked steel modular cabins used in energy infrastructure construction. Modular construction offers significant benefits, including increased construction efficiency, reduced environmental impact, and improved safety. However, the seismic performance of modular structures presents unique challenges, particularly in earthquake-prone regions. To address these challenges, the paper presents a reinforcement method that incorporates corrugated steel plate walls at key structural locations, particularly at the lower corners of the ground floor. This approach is designed to improve lateral stiffness and energy dissipation without compromising construction simplicity or cost effectiveness. Finite Element Analysis (FEA) was used to evaluate the effectiveness of this method and demonstrated significant improvements in seismic performance. The results indicate that the proposed reinforcement reduces stress concentrations and mitigates interstory drift, thereby improving the overall structural resilience of the modular assemblies under seismic loading. The results provide a promising solution for balancing structural performance, ease of construction, and economic considerations in the context of seismic reinforcement for modular infrastructure.

Keywords: corrugated steel plate walls, finite element analysis, modular construction, power infrastructure, seismic reinforcement

[1]PhD., Eng., State Grid Anhui Electric Power Co., Ltd., No.133, Susong Road, Baohu District Hefei, China, e-mail: liuzhixiang6150@163.com, ORCID: 0009-0006-0117-0062
[2]PhD., Eng., State Grid Anhui Electric Power Co., Ltd., No.133, Susong Road, Baohu District Hefei, China, e-mail: jinxingfu6150@163.com, ORCID: 0009-0006-2505-8884
[3]PhD., Eng., State Grid Anhui Electric Power Co., Ltd., No.133, Susong Road, Baohu District Hefei, China, e-mail: muhong6150@163.com, ORCID: 0009-0001-8080-7685
[4]PhD., Eng., Department of Structural Engineering, Tongji University, No.1239, Siping Road, Yangpu District Shanghai, China, e-mail: yangbo0815@tongji.edu.cn, ORCID: 0009-0004-1819-0540

1. Introduction

Modular structures offer significant advantages over traditional forms, including increased construction efficiency, higher standardization, reduced labor, lower carbon emissions [1,2], and improved safety and reliability, making them highly suitable for the industrialization of new construction [3,4]. Their effectiveness is particularly evident in complex environments with limited space and constrained conditions, offering promising potential for infrastructure projects [5].

In energy infrastructure, modular construction has unique strengths. Standardized design, factory fabrication, and modular assembly effectively address the challenges of large-scale power grid projects, such as extra- high voltage systems [6]. Modular facilities shorten construction cycles and improve safety and quality, especially by modularizing substations and generator houses, while facilitating future expansion and maintenance [7].

As China is located in a seismic area, the evaluation of the seismic performance of modular structures is critical [8]. Their dynamic response under seismic loads differs from conventional structures due to module connections and assembly characteristics, revealing the limitations of traditional seismic design methods [9].

Research on the seismic performance of modular structures is extensive. Annan et al. [10,11] conducted static tests on a multi-story modular steel frame and found different modes of vibration. Hong et al. [12] studied a modular unit frame with corrugated steel plates that effectively dissipated seismic energy. Fathieh [13, 14] identified maximum interstory displacement angles as reliable vulnerability indicators.

To improve seismic resistance, scholars have proposed various solutions. Fan [15] proposed a dual-module system for gravity and lateral forces, while Chen et al. [16] investigated a modular bollard-braced frame with damping mechanisms. Jing [17] recommended passive energy-dissipating sliders, and Feng [18] developed a thick-walled steel modular system to increase load capacity.

Despite improvements, challenges remain in terms of design complexity and cost, especially in seismic regions, making it difficult to balance performance and cost. Therefore, it is essential to explore more compact and efficient seismic strengthening methods.

This paper proposes a compact seismic strengthening method for stacked steel modular chambers in energy infrastructure that optimizes structural layouts and material usage, while enhancing inter-module connections to ensure robust seismic performance.

2. Building structure layout

When using modular construction in electrical infrastructural facilities, a number of space-demanding electrical equipment are installed in the modular cabin before the cabins are assembled onsite. Shown in Fig. 1(a) are some demonstrative equipment installed in the modular cell (cabin). In Fig. 1(b), an equipment-modular integration that are ready for transportation is presented. Due to the large and flexible opening demand on the cabin wall, the vertical structural members, i.e., columns or column-walls, should be compact, architecturally low-invasive, and strong. Since there is no space for bracing (interfering wall-openings), the lateral stiffness demand on the columns (standing at the corners) becomes pronounced.

(a) (b)

Fig. 1. (a) Space-occupying equipment installed in modular cabin; (b) Equipment-modular integration with large flexible wall-openings

Corrugated steel plate walls and columns are specially designed steel plate walls with a regular corrugated shape on the surface of the steel plate to increase its rigidity and load carrying capacity. Compared with traditional flat steel walls, the geometry of the corrugated steel plate provides better resistance to lateral loads during loading, as well as greater bending and shear resistance to external forces such as earthquakes. The corrugated design not only increases the critical buckling load of the steel plate, but also improves the energy dissipation capacity of the overall structure, making it more resilient and stable under extreme conditions such as earthquakes. This type of reinforcement is particularly suitable for providing additional support in weak areas of the structure. As shown in Fig. 2, in the existing modular box stacking systems, corrugated steel wall columns are installed at the lower corners, which can effectively increase the lateral deformation resistance in this area. As the corner is usually the area where the force is concentrated under seismic action, the installation of corrugated steel plate wall columns can greatly reduce the lateral displacement in this area, thus preventing the risk of collapse or serious deformation of the whole structure due to corner instability.

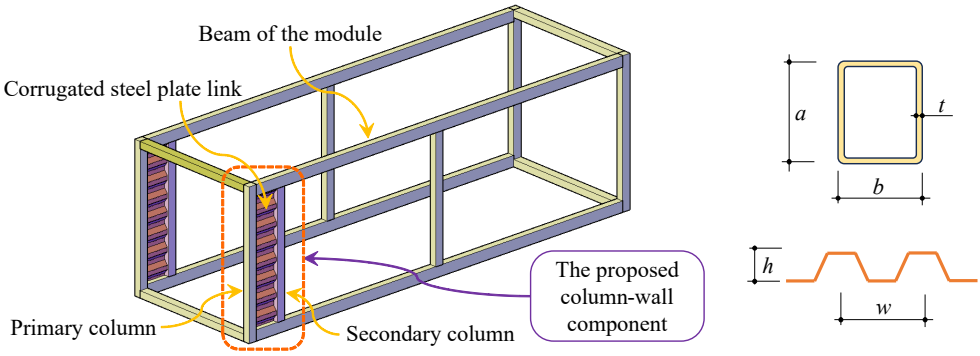

Fig. 2. Configuration of the proposed column-wall component of the module

The cross-sectional dimensions of the components of the module are shown in Table 1. The base and top slabs of the modules were modelled with in-plane diagonal bracing.

Table 1. Cross-sectional Dimensions of Modular Components

Modular column	**Bottom beam**		**Top beam**		**Foundation Column**
	Longitudinal	Cross	Longitudinal	Cross	
180×180×6	150×100×6	200×100×6	100×100×6	100×100×6	200×200×6

The proposed column-wall component is shown in Fig. 2, which consists of a primary tubular column (with a larger sectional size), a secondary tubular column (with a smaller sectional size), and a corrugated steel plate link in between. The primary column, the secondary column and the corrugated plate in the configuration shown in Fig. 2 are welded with each other. In this proposal, the axial load of the coupled member mainly acts on the primary column, while the lateral load-stiffness and energy-dissipation are provided by all three elements together (primary and secondary columns, and their corrugated link).

To accommodate various structural and functional requirements, two distinct module arrangement schemes were developed, and the corresponding 3D models and seismic reinforcement strategies for each stacking structure program are shown in Fig. 3.

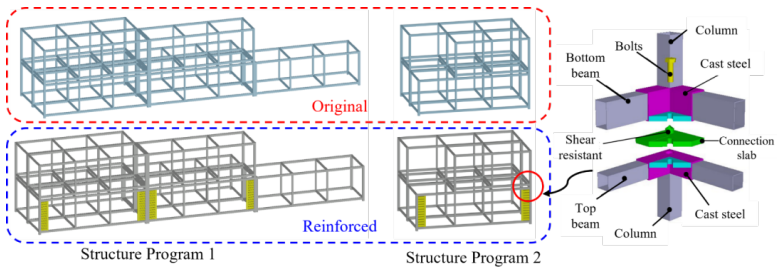

Fig. 3. Modular stacking and corresponding reinforcement structure program

3. Modelling the column-wall component on the ANSYS platform

3.1. Parametrical FEM modelling scheme

In this research, the geometries of the members in a column-wall component are set in compliance with a steel modular electric substation (as shown before in Fig. 2). The height, width, and length of a module is set to H = 3.5 m, W = 3.5 m, and L = 11.5 m, respectively, which is shown in Fig. 4. The cross sections of the tubular members (columns and beams) and the corrugated steel plate link, denoted in Fig. 4, alter within a reasonable range.

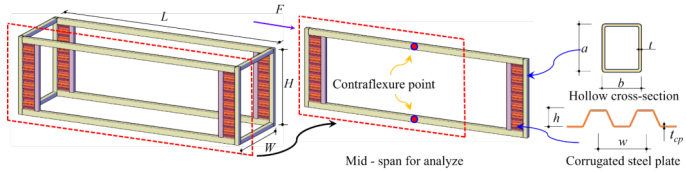

Fig. 4. Equivalence of engineering and analytical models

Three degrees of vertical load, measured by the compression ratio η, are considered in the lateral hysteretic response simulation. Here η is defined by

$$\eta = n/A_{pc}f_y \tag{3.1}$$

where N is the vertical compression acting on the primary column, A_{pc} is the cross-sectional area of the primary column, and f_y is the yield strength of steel. In this work, we use $f_y = 235$ MPa and consider $\eta = 0.20$, 0.25, and 0.30.

The primary column and the beams in the specimens were fabricated by Q345B steel, while the corrugated steel plate and secondary column were constructed from Q235B steel. The material properties were calibrated through standard coupon tests. According to the test, we take $f_y = 362$ MPa for the primary- and the secondary-column, and $f_y = 277$ MPa for the corrugated steel plate link. The model proposed by Shi et al. [19] was used to simulate the hysteretic behaviour of the steel. The backbone curves of steel are shown in Eq. (3.2):

$$\frac{\sigma}{\sigma_y} = \begin{cases} \dfrac{\varepsilon}{\varepsilon_y}; & \left(\dfrac{\varepsilon}{\varepsilon_y} < 1\right) \\ \dfrac{\left(\dfrac{\varepsilon}{\varepsilon_y} + a_0\right)}{b_0 + b_1\left(\dfrac{\varepsilon}{\varepsilon_y} + a_0\right) + b_2\left(\dfrac{\varepsilon}{\varepsilon_y} + a_0\right)^2}; & \left(\dfrac{\varepsilon}{\varepsilon_y} \geq 1\right) \end{cases} \tag{3.2}$$

The SHELL181 element of the ANSYS platform is used to simulate thin-walled steel members in column-wall assemblies. Geometric nonlinearities are fully taken into account in the simulation. The column bases are simulated with rigid constraints. Beams are simulated using a half-model where the beam mid-span is pinned. The connections between components are rigid as they are structurally welded. After applying the vertical load, a hysteretic lateral loading process is conducted. Established FEM and loading protocol are illustrated in Fig. 5.

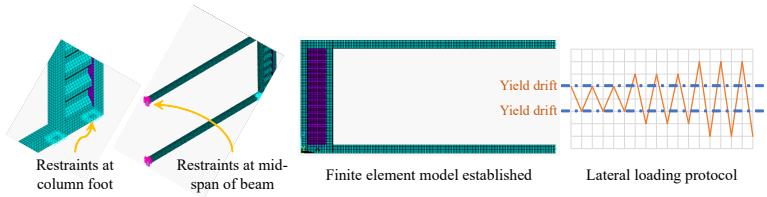

Fig. 5. Illustrative finite element model and the lateral loading protocol

The loading protocol contains three loops at an inter-story drift of d_y, $2d_y$, and $3d_y$, respectively. Here d_y corresponds to the point where a 1% increment of load give rise to a 2% or more reduction in the tangent stiffness of the load-displacement curve.

3.2. Hysteretic property of the column-wall component

The obtained hysteretic loops of the 20 finite element models are shown in Fig. 6, respectively, corresponding to the two different types of primary column, namely, $a \times b \times t$ = 200×200×8 mm. The corrugated plate is $w \times h \times t_{cp}$ = 240 × 60 × 2 mm for Model 1–14, $w \times h \times t_{cp}$ = 240×60×3 mm for Model 1–18, and $w \times h \times t_{cp}$ = 240×60×2.5 mm for the rest. Note that all models exhibited a stable post-yield behavior, and the strength degrading is not quite pronounced. This proves the good hysteretic performance of the proposed column-wall component. And D is the distance between the centre lines of the primary and secondary columns.

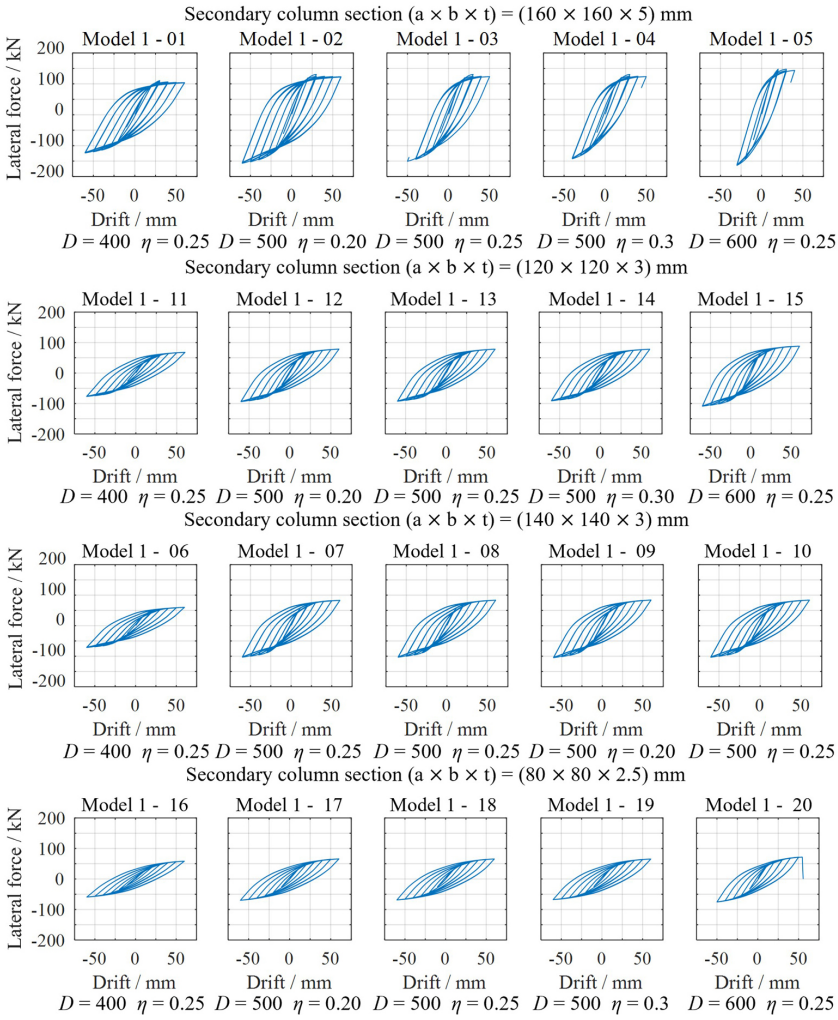

Fig. 6. Hysteretic loops of column-wall components with primary column size 200×200×8 mm

3.3. Influence of member geometry

Altering the axial distance between the primary and the secondary column from 400 mm to 600 mm, the strength of the column-wall is increased, and the degree of an-symmetry of the hysteretic loop gets pronounced. However, an enlarged value of D may weaken the deforming ability of the column-wall, as shown in Model 1-01, 1-03, and 1-05. This is because a larger D generates an amplification of the equivalent moment of inertia of the column-wall section.

From the results of Model 1-09, Model 1-10, Model 1-16, 1-17 and 1-18, the thickness of corrugated steel plate link basically has no influence on the hysteretic performance of the column-wall.

Observing the results of Model 1-03, 1-08, 1-12 and 1-17, a smaller secondary column gives a decrease in the strength and stiffness of the column-wall.

4. Modelling the modular structure on the ANSYS platform

4.1. Influence of member geometry

The incorporation of corrugated steel plate wall-column assemblies into structures and the subsequent evaluation of their seismic performance can be effectively conducted through the use of refined modelling techniques, such as the SHELL181 method. This approach allows for the accurate representation of the mechanical behaviour of the members; however, it is typically accompanied by elevated computational costs and presents challenges in terms of flexible reinforcement site selection, which can impede the conduct of parametric analysis. Accordingly, this paper proposes an alternative approach, defining a new material model. This method achieves equivalence in seismic performance by modifying the cross-section shape and stiffness parameters of the material and establishing a specific constitutive relationship, thereby aligning the hysteresis characteristics of the simplified rectangular column cross-section with those of the original member. This approach markedly reduces the computational complexity while maintaining the essential characteristics of the structural performance. Figure 7 illustrates the comparison of the hysteretic performance of the equivalent wall and column, with the corrugated plate is $w \times h \times t_{cp} = 240 \times 60 \times 2.5$ mm.

Figure 7 illustrates the comparative analysis of the hysteresis performance of the equivalent walls and columns with the original members across different parameter groups. In general, the hysteresis curves of the various groups of equivalent models are largely consistent with the hysteresis behaviours of the original members, particularly Model – A to Model – F, which have highly satisfactory simulation results in terms of peak load, displacement amplitude, and energy dissipation capacity. By making reasonable adjustments to the width of the corrugated plate and the size ratio of the main column and sub-column, these models are able to successfully achieve a high degree of restoration of the hysteretic behaviour, indicating that the equivalent models are capable of effectively simulating the seismic characteristics of the actual members.

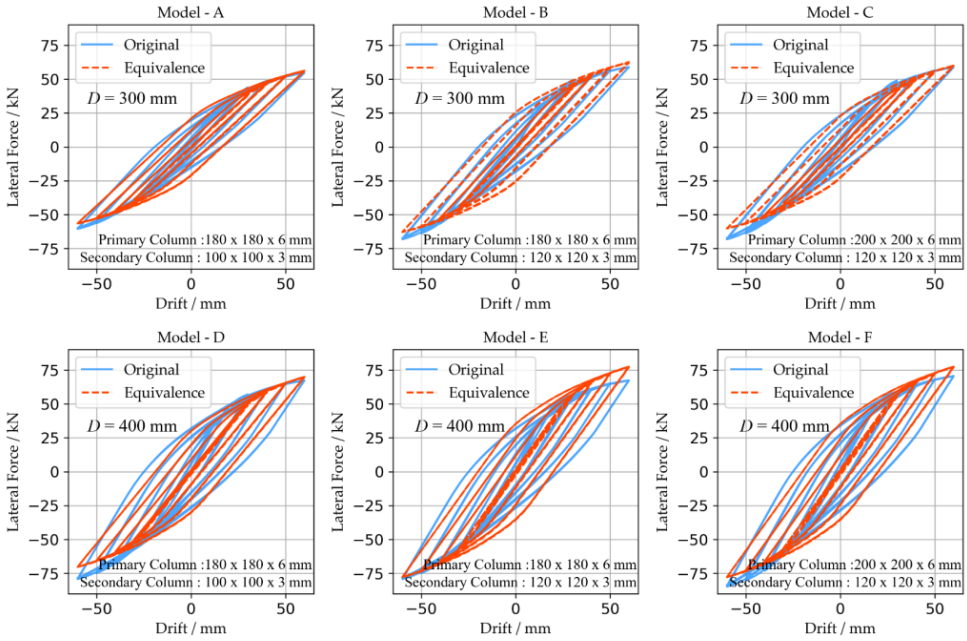

Fig. 7. Comparison of hysteretic performance of equivalent wall and columns

4.2. Structural modelling method

This model primarily utilizes BEAM188 and COMBIN14 elements to simulate the structural response. The transverse and longitudinal beams within the box structure are represented through beam and rod elements. The concentrated masses at the key nodes are applied following the guidelines specified in the seismic design code [20].

The boundary conditions and loads applied in the three finite element models for the stacked configuration are shown in Fig. 8. In this figure, the green segments represent the coupling between elements, the blue segments represent the beam-column elements, 'M0' denotes the mass elements, the yellow sections at the column bases indicate boundary constraints, and the light blue sections represent the COMBIN14 elements, used to simulate the in-plane stiffness of the floor slab in the actual structure.

To account for energy dissipation during dynamic analysis, Rayleigh Damping was applied in this study. This method expresses the damping matrix C as a linear combination of the mass matrix M and stiffness matrix K:

$$C = \alpha M + \beta K \tag{4.1}$$

where α and β are the mass- and stiffness-proportional coefficients. These coefficients were determined based on the first two natural frequencies and a target damping ratio of 5%.

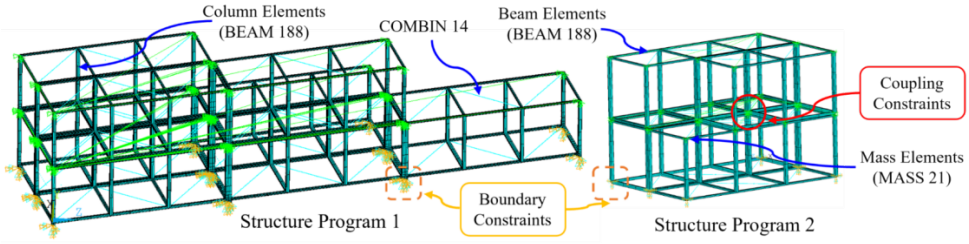

Fig. 8. Finite element modelling

4.3. Dynamic property of the modular structures

4.3.1. Vibrating period

Modal analyses were performed for two different module stacking configurations. Only the natural frequencies of the first two modes are reported, as the higher-order modes exhibited negligible participation factors. The results clearly show an increase in the fundamental frequency of the reinforced structure, regardless of the stacking configuration. This indicates an enhancement in the overall stiffness of the strengthened structure, leading to a reduction in lateral displacements of both structural and non-structural components under seismic loads.

4.3.2. Vibrating mode

As illustrated in Fig. 9 and Fig. 10, the results of the modal analysis for the modular stacked structure program 1 and the stacked structure program 2 reveal that, in the case of structure program 1, there is no significant change in the modal state of the structure before and after the reinforcement. This finding indicates that the reinforcement exerts minimal influence on the structural modes, and the original dynamic characteristics remain largely unaltered. The frequency of the structure is reduced after reinforcement, and the overall stiffness is significantly increased. The structure exhibits a faster return to equilibrium and enhanced resistance to deformation when subjected to the same external load.

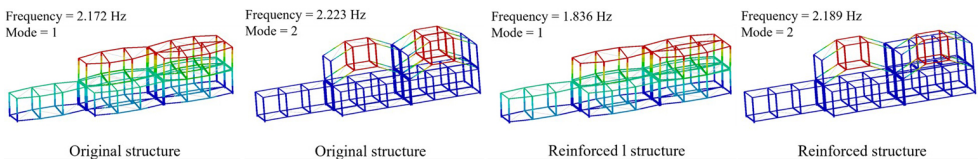

Fig. 9. The first two orders of vibration modes of structure program 1

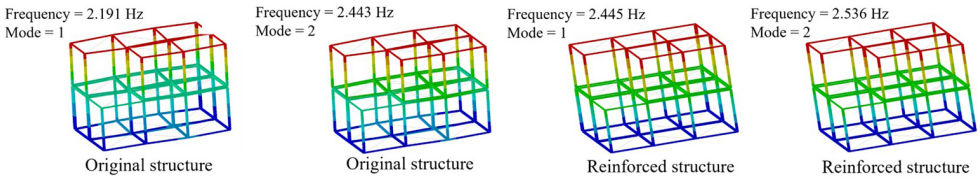

Fig. 10. The first two orders of vibration modes of structure program 2

5. Seismic performance of (reinforced) modular structures

5.1. Earthquake input

The artificial seismic waves used in this study are generated based on standard spectral theory, utilizing the Kiyoshi Kanai power spectrum model as the target spectrum [21]. The aim is to produce artificial acceleration time histories, assuming that all ground motions can be decomposed into a series of trigonometric functions with varying periods. An iterative method is used to compute the power spectral density function from the input spectral data. The Fourier amplitude spectrum is then derived from the power spectrum. Finally, the Fourier inversion technique is applied to generate smooth seismic acceleration time histories. The resulting 50 artificial wave acceleration power spectra are illustrated in Fig. 11. S_a is the absolute acceleration spectrum of the structure and g is the gravitational acceleration.

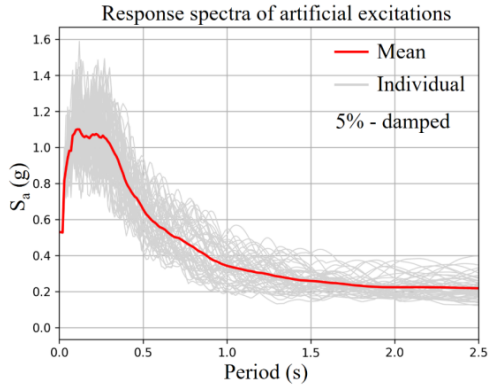

Fig. 11. Response spectra of artificial excitations

Parameters are established in accordance with the Code for Seismic Design of Buildings (GB50011-2010) [22], adopting varying peak accelerations of seismic waves to meet specific design requirements. This paper employs the proportional adjustment method for amplitude correction. The selected structural intensity is 8-degree (0.2 g), with maximum seismic acceleration values set at 70 cm/s^2 for minor earthquakes, 196 cm/s^2 for moderate earthquakes, and 400 cm/s^2 for rare earthquakes. The acceleration time histories of the seismic waves are adjusted to 70, 150, 196, 300, and 400 cm/s^2.

Figure 12 and Fig. 13 present the comparative analysis of maximum stress, inter-story displacement, and inter-story acceleration of the structure before and after reinforcement for stacking structure program 1 under the influence of the 28th artificial wave. Prior to reinforcement, the maximum stress in the structure was 304 MPa, approaching the yield strength of the material, indicating a significant risk of local plastic deformation under intense seismic activity. After reinforcement, the maximum stress decreased to 234 MPa, reflecting a 23% reduction. This reduction demonstrates that the reinforcement measures effectively alleviated stress concentration issues, thereby improving the seismic performance of the structure.

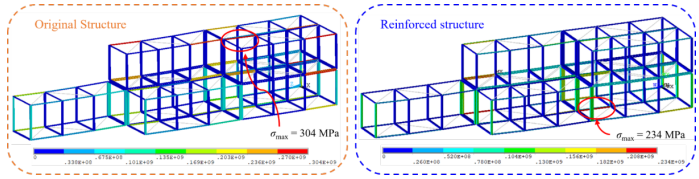

Fig. 12. Peak stress comparison

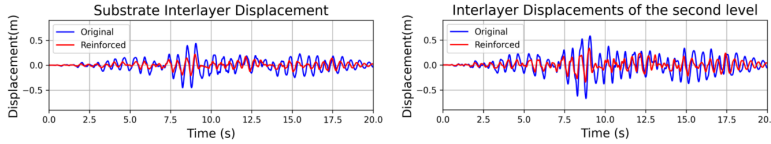

Fig. 13. Comparison of interlayer displacement

Figure 13 demonstrates a significant reduction in relative inter-story displacements for both the one- and two-story structures, with the most notable decrease occurring at the ground floor. This result highlights the effectiveness of the reinforcement measures in enhancing the overall stiffness of the structure and reducing inter-story displacement responses.

5.2. Structural vulnerability analysis

The seismic damage condition of a structure is categorized into five grades based on the extent of damage sustained during an earthquake: intact, slight damage, moderate damage, severe damage, and collapse. The transitional state between these grades, known as the limit state, represents the performance level of the structure. This level indicates the maximum degree of damage that the structure may experience under a specific level of seismic loading. In this study, the maximum inter-story displacement angle is used as the damage index, with the evaluation criteria for the ultimate state detailed in Table 2.

Table 2. Structural limit state definitions

Performance Levels	**Basically intact**	**Slight damage**	**Moderate damage**	**Severe damage**	**Destruction**
Extreme state	LS_1	LS_2	LS_3	LS_4	LS_5
Interstory DriftAngle Limit	1/600	1/400	1/200	1/100	1/50

The seismic susceptibility of a structure can be defined as the probability that the seismic demand of a structure or member exceeds the seismic capacity under seismic action. This probability-based method of assessing the seismic performance of a structure can be expressed as follows [22]:

$$P_f\left[L_s \mid IM = y\right] = P\left[C \le D \mid IM = y\right] \tag{5.1}$$

In Eq. (5.1), P_f is the damage exceedance probability of the structure at different ground motion intensities, IM is the ground motion intensity parameter, and y is the specific value of the different ground motion intensity parameters. The location of the aforementioned item is as follows: In this context, L_s represents the limit state, C denotes structural capacity, and D signifies structural demand. It is typically assumed that C and D are two independent random variables, both of which follow a lognormal distribution. In this case, the aforementioned equation can be transformed into:

$$P_f = \Phi\left(\frac{\ln S_d - \ln S_c}{\sqrt{\beta_d^2 + \beta_c^2}}\right) \tag{5.2}$$

In Eq. (5.2), Φ denotes the standard normal distribution function; S_d denotes the mean value of structural demand, and S_c denotes the mean value of structural capacity; β_d is the log standard deviation of structural demand; and β_c is the log standard deviation of structural capacity. The value of β_d is obtained according to the seismic demand model, and β_c is set to 0.3 [23]. Substitution of the relational equation between ground shaking intensity and structural demand, derived from the IDA method, into the equation for the damage exceeding probability of the box structure under different ground shaking intensities allows for the calculation of this probability. Figure 14 depicts the vulnerability curves for two different stacking structures.

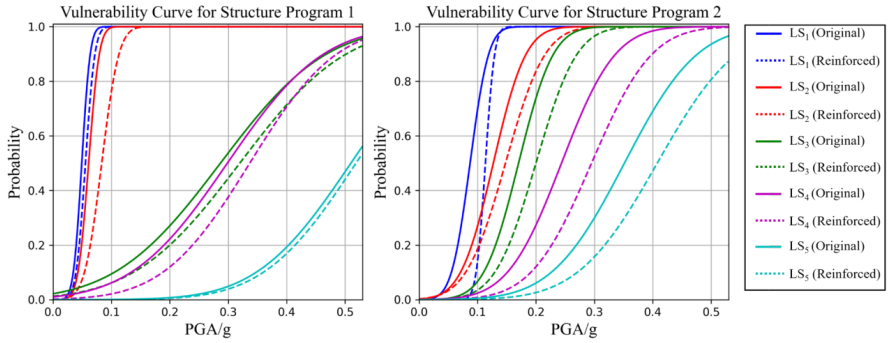

Fig. 14. Stacking vulnerability curve

In Fig. 14, PGA is peak ground acceleration in units of gravitational acceleration. The dashed lines represent the vulnerability curves after reinforcement, while the solid lines show the curves for the structures without reinforcement. The vulnerability curves of the reinforced structure

are shifted to the right compared to the original structure, signifying a reduced probability of failure across various damage states due to the reinforcement measures. This indicates that the seismic capacity of the box structure is significantly improved following reinforcement.

In the case of modular stacking structure program 1, when $IM < 0.1$, it can be observed that the structures of the boxes that were subjected to reinforcement have sustained slight damage, which may be attributed to the inherent asymmetry of the structure program 1. As the value of IM gradually increases, it can be seen that the probability of the structure that has undergone reinforcement sustaining moderate damage, severe damage, or complete destruction gradually decreases.

In the case of modular stacking structure program 2, when $IM < 0.1$, the probability of each damage state of the box structure is essentially zero. When $0.2 < IM < 0.4$, the probability of each stage of damage of the box structure rises significantly. After reinforcement, the probability of each damage state occurring under the same ground vibration intensity parameters decreases significantly.

The above susceptibility curves demonstrate that the implementation of reinforcement measures can markedly enhance the seismic resilience of the structure. The reinforced structure exhibits robust stability and a minimal risk of collapse under the intensity of 7- and 8-degree rare earthquakes, thereby exhibiting excellent seismic potential.

6. Conclusions

This paper introduces a passive energy dissipation and seismic strengthening method specifically designed for low and medium-rise prefabricated steel frame structures. This method is applied to the seismic analysis of two representative box-stacked steel frame configurations. The study assesses the feasibility and effectiveness of the method by comparing the seismic susceptibility of the structures before and after reinforcement across all two stacking schemes. In addition, a parametric analysis was conducted on corrugated steel plate column-wall structures to evaluate the influence of key parameters.

1. The column-wall assembly system presented in this study, featuring a high aspect ratio and ease of construction, is particularly well-suited for modular buildings. It offers spatial efficiency and flexibility in accommodating a variety of functional wall openings. Its simple construction process and demonstrated effectiveness in improving seismic performance make it an ideal solution for modular structures. Additionally, the system simplicity and versatility position it as a promising option for improving the seismic performance of modular buildings in practical engineering applications.
2. The distance between the main column and sub-column has been shown to have a significant impact on the seismic performance of the structure. It has been demonstrated that increasing the distance between the main column and sub-column results in a corresponding increase in the structural rigidity. However, it is imperative to exercise caution when determining the optimal distance between the main column and sub-column, as an excessively large distance may result in an asymmetric hysteresis curve. The thickness of the corrugated steel plate exerts minimal influence on the seismic

performance of the structure. In the practical application of the project, it is imperative to establish the value of D and ensure that the sub- column cross-section size is not reduced to an excessively small dimension.

3. The passive energy dissipation and seismic strengthening method proposed for low- and medium-rise prefabricated steel frame structures achieves the expected seismic performance improvements. The proposed design approach is practical and effective, as evidenced by the substantial reduction in seismic response and damage across all evaluated states. This demonstrates the method's capability to enhance structural resilience and reduce vulnerability to earthquake-induced damage.

Acknowledgments

The present work was supported by the Science and Technology Project of State Grid Corporation of China (Grant No. 5200-202320127A-1-1-ZN), which is gratefully appreciated.

References

[1] A. Tofiluk, "Problems and challenges of the built environment and the potential of prefabricated architecture", *Archives of Civil Engineering*, vol. 69, no. 3, pp. 405–424, 2023, doi: 10.24425/ace.2023.146088.

[2] J. Pasławski and K. Włoch-Surówka, "Modular construction in adapting to changing requirements on the example of railway stations", *Materiały Budowlane*, vol. 2023, no. 1, pp. 4–9, 2023, doi: 10.15199/33.2023.01.02 (in Polish).

[3] N. Boyd, M.M.A. Khalfan, and T. Maqsood, "Off-Site Construction of Apartment Buildings", *Journal of Architectural Engineering*, vol. 19, no. 1, pp. 51–57, 2013, doi: 10.1061/(ASCE)AE.1943-5568.0000091.

[4] W. Ferdous, Y. Bai, T.D. Ngo, A. Manalo, and P. Mendis, "New advancements, challenges and opportunities of multi-storey modular buildings – A state-of- the-art review", *Engineering Structures*, vol. 183, pp. 883–893, 2019, doi: 10.1016/j.engstruct.2019.01.061.

[5] R.M. Lawson, R.G. Ogden, and R. Bergin, "Application of Modular Construction in High-Rise Buildings",*Journal of Architectural Engineering*, vol. 18, no. 2, pp. 148–154, 2012, doi: 10.1061/(ASCE)AE.1943-5568.0000057.

[6] "The National Energy Administration organized the release of the 'Blue Book on the Development of New Power Systems", *iEnergy*, vol. 2, no. 2, pp. 87–88, 2023, doi: 10.23919/IEN.2023.0017.

[7] H. Guo, C. Ma, and Z. Wen, "Key technologies and prospects of prefabricated modular substations", *Electrical Technology*, vol. 24, no. 9, pp. 1–10, 19, 2023, doi: 10.3969/j.issn.1673-3800.2023.09.001.

[8] Y. Jiaolong and F. Ruikai, "Analysis of the current application status of prefabricated steel structures in China", *Engineering Construction and Design*, no. 17, pp. 13–15, 2020, doi: 10.13616/j.cnki.gcjsysj.2020.09.005.

[9] B. Zhao, D. Wu, and H. Zhu, "New modular precast composite shear wall structural system and experimental study on its seismic performance", *Engineering Structures*, vol. 264, art. no. 114381, 2022, doi: 10.1016/j.engstruct.2022.114381.

[10] C.D. Annan, M.A. Youssef, and M.H. El Naggar, "Seismic Vulnerability Assessment of Modular Steel Buildings", *Journal of Earthquake Engineering*, vol. 13, no. 8, pp. 1065–1088, 2009, doi: 10.1080/13632460902933881.

[11] C.D. Annan, M.A. Youssef, and M.H. El Naggar, "Experimental evaluation of the seismic performance of modular steel-braced frames", *Engineering Structures*, vol. 31, no. 7, pp. 1435–1446, 2009, doi: 10.1016/j.engstruct.2009.02.024.

[12] S.-G. Hong, B.-H. Cho, K.-S. Chung, and J. Moon, "Behavior of framed modular building system with double skin steel panels", *Journal of Constructional Steel Research*, vol. 67, no. 6, pp. 936–946, 2011, doi: 10.1016/j.jcsr.2011.02.002.

[13] A. Fathieh and O. Mercan, "Seismic evaluation of modular steel buildings", *Engineering Structures*, vol. 122, pp. 83–92, 2016, doi: 10.1016/j.engstruct.2016.04.054.

[14] A. Fathieh and O. Mercan, "Three-Dimensional, Nonlinear, Dynamic Analysis of Modular Steel Buildings", in *Structures Congress 2014.* Boston, MA, USA: American Society of Civil Engineers, 2014, pp. 2466–2477, doi: 10.1061/9780784413357.216.

[15] G. Fan, J. Men, Y. Fu, T. Lan, and J. Wang, "Seismic behavior of steel plate wall with stiffeners and concrete slab in the box-plate steel structure", *Journal of Building Engineering*, vol. 69, art. no. 106239, 2023, doi: 10.1016/j.jobe.2023.106239.

[16] L. Chen, R. Tremblay, and L. Tirca, "Seismic Performance of Modular Braced Frames for Multi-Storey Building Applications", presented at 15th World Conference on Earthquake Engineering, Lisbon, Portugal, 24–28 Sep. 2012.

[17] J. Jing, "Seismic Damage-Resistant System for Modular Steel Structures", PhD dissertation, Auckland, 2016. [Online]. Available: https://www.researchgate.net/publication/362567819_Seismic_Damage-Resistant_System_for_Modular_Steel_Structures.

[18] R. Feng, L. Shen, and Q. Yun, "Seismic performance of multi-story modular box buildings", *Journal of Constructional Steel Research*, vol. 168, art. no. 106002, 2020, doi: 10.1016/j.jcsr.2020.106002.

[19] Y. Shi, M. Wang, and Y. Wang, "Experimental and constitutive model study of structural steel under cyclic loading", *Journal of Constructional Steel Research*, vol. 67, no. 8, pp. 1185–1197, 2011, doi: 10.1016/j.jcsr.2011.02.011.

[20] GB/T 7714-2015 Code for Seismic Design of Buildings. The Ministry of Housing and Urban-Rural Development of the PRC, 2016.

[21] Y. Liang, C. Xiao, T. Wu, Z. Xu, and J. Fan, "Artificial earthquake wave synthesis based on building code response spectrum and its application", *Journal of Sichuan University of Science and Engineering (Natural Science Edition)*, vol. 29, no. 5, pp. 83–87, 2016, doi: 10.11863/j.suse.2016.05.18.

[22] Y. Lieping, M. Qianli, and M. Zhiwei, "Study of seismic intensity indices for structural seismic analysis", *Earthquake Engineering and Engineering Vibration*, vol. 29, no. 4, pp. 9–22, 2009, doi: 10.13197/j.eeev.2009.04.019.

[23] Y.K. Wen, B.R. Ellingwood, D. Veneziano, and J. Bracci, "Uncertainty Modeling in Earthquake Engineering", 2003.

Received: 2024-09-19, Revised: 2025-01-12